NANO LETTERS

Letter

pubs.acs.org/NanoLett

Novel p-Type Conductive Semiconductor Nanocrystalline Film as the Back Electrode for High-Performance Thin Film Solar Cells

Ming-Jian Zhang, Qinxian Lin, Xiaoyang Yang, Zongwei Mei, Jun Liang, Yuan Lin, and Feng Pan*

School of Advanced Materials, Peking University Shenzhen Graduate School, Shenzhen 518055, China

Supporting Information

ABSTRACT: Thin film solar cells, due to the low cost, high efficiency, long-term stability, and consumer applications, have been widely applied for harvesting green energy. All of these thin film solar cells generally adopt various metal thin films as the back electrode, like Mo, Au, Ni, Ag, Al, graphite, and so forth. When they contact with p-type layer, it always produces a Schottky contact with a high contact potential barrier, which greatly affects the cell performance. In this work, we report for the first time to find an appropriate p-type conductive semiconductor film, digenite Cu_9S_5 nanocrystalline film, as the back electrode for CdTe solar cells as the model device. Its low sheet resistance (16.6 Ω/sq) could compare to that of the commercial TCO films (6−30 Ω/sq), like FTO, ITO, and AZO. Different from the traditonal metal back electrode, it produces a successive gradient-doping region by the controllable Cu diffusion, which greatly reduces the contact potential barrier. Remarkably, it achieved a comparable power conversion efficiency (PCE, 11.3%) with the traditional metal back electrode (Cu/Au thin films, 11.4%) in CdTe cells and a higher PCE (13.8%) with the help of the Au assistant film. We believe it could also act as the back electrode for other thin film solar cells (α-Si, $CuInS_2$, CIGSe, CZTS, etc.), for their performance improvement.

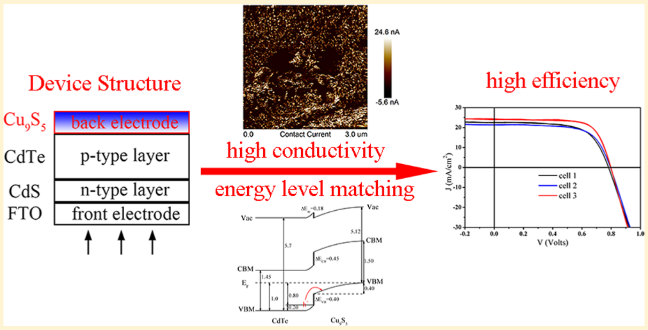

KEYWORDS: *p-Type conductive semiconductor film, Cu_9S_5 nanocrystal, back electrode, thin film solar cells, high electrical conductivity, energy level matching*

The well-known thin film solar cells includes α-Si,[1,2] CdTe,[3−5] $CuInS_2$,[6,7] $Cu(In,Ga)Se_2$ (CIGSe),[8] $Cu_2ZnSn(S,Se)_4$ (CZTS)[9] and so forth. For thin film solar cells, efficiency improvement and cost reduction are always two main goals. Generally, the common methods for improving efficiencies includes designing new device structures,[2,10−12] improving the material composition and related crystalline quality of thin films,[13−15] optimizing the contact interfaces between thin films.[16−18] From the view of the device structure (front electrode/n-type layer/p-type layer/back electrode), the front electrode is usually adopting kinds of n-type transparent conductive oxide (TCO) films, like FTO, ITO, and AZO, aiming to collect and transport photon-generated electrons. Correspond to these n-type TCO films as the front electrode, adopting p-type conductive semiconductor films as the back electrode should be a good choice to collect and transport photon-generated holes. Actually, all thin film solar cells now generally adopt kinds of metal thin films as the back electrode, like Mo, Au, Ni, Ag, Al, and so forth. This is due to the scarcity of p-type conductive semiconductors and the mature preparation technology of various metal thin films. However, the disadvantage of using of these metal thin films as back electrodes is to form a Schottky contact between itself and the p-type layer with a high contact potential barrier, which greatly affects the cell efficiency.

This problem is particularly acute for CdTe thin film solar cells, which are most popular with biggest marketing share in thin film solar cell industry. Owing to itself intrinsic high work function (5.7 eV) of CdTe material, commonly used high work functional metal back electrodes, including Au, Ni, Mo, graphite and etc., are hard to produce a good Ohmic contact with CdTe layer. To solve this problem, the sole strategy is introducing some special back contacts, such as Cu thin film, ZnTe:Cu,[19,20] Sb_2Te_3,[21] MoO_3,[22,23] and etc., to reduce the contact potential barrier between the metal back electrode and p-type semiconductor CdTe layer. But the introducing of these special materials not only raise the cost issues because of their complex preparation process, but also bring more uncontrollable parameters into the continuous production of high-performance CdTe thin film solar cells. For example, efforts have been devoted to introducing Cu into CdTe layer to form Ohmic back contact for improving the cell performance.[24−27] However, the diffusion degree of Cu strongly depends on the deposition thickness of Cu thin film, the annealing temperature and the annealing time. Excessive amount of free Cu always diffuse through CdTe layer into the underlying CdS layer, which results in a "roll-over" phenomena of J-V curve and

Received: November 5, 2015
Revised: December 19, 2015
Published: January 6, 2016

DOI: 10.1021/acs.nanolett.5b04510
Nano Lett. 2016, 16, 1218−1223

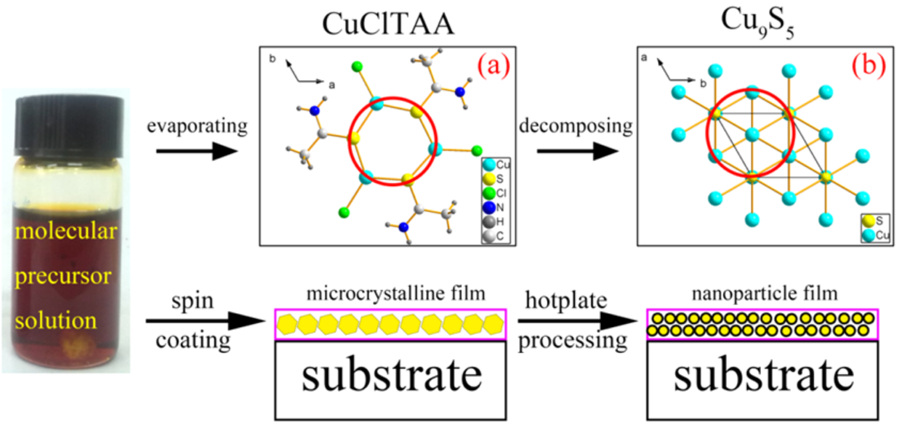

Figure 1. Schematic diagram for the preparation process of Cu_9S_5 nanoparticle condutive thin film; (a) the crystal structure of CuClTAA; (b) the crystal structure of Cu_9S_5.

greatly reduces the cell performance.[28,29] In one word, development of novel back electrode, especially p-type conductive semiconductor with a good Ohmic contact, is essential for the improvement of the cell performance in thin film solar cells.

In this work, we report for the first time to develop an appropriate p-type conductive semiconductor film, digenite Cu_9S_5 nanocrystal,[30] as the back electrode for CdTe solar cells as the model device, which could be a new back electrode candidate to apply for other thin film solar cells. We develop a facile molecular precursor solution method to fabricate Cu_9S_5 nanocrystalline conductive film. Its low sheet resistance could compare to the commercial TCO films, like FTO, ITO, and AZO, showing it could be used for the back electrode to collect and transport holes. Moreover, it produces a successive gradient-doping region by the controllable Cu diffusion, which greatly reduces the contact potential barrier. Finally, it achieved about 2.4% higher power conversion efficiency (PCE, 13.8%) with Cu_9S_5 nanocrystalline conductive film as the back electrode than that of the traditional metal back electrode (Cu/Au thin films, 11.4%) in CdTe solar cells, which mainly results from the improvement of fill factors (FFs) with the favorable energy level matching of CdTe/Cu_9S_5 interface forming by the Cu gradient diffusion.

To apply Cu_9S_5 as the back electrode in thin film solar cells, the process for preparing high quality thin film must be investigated at first. Herein, we develop a facile molecular precursor solution method to prepare its thin film for the first time (Figure 1). At first, a molecular precursor solution was prepared by dissolving $CuCl_2$ and thioacetamide (TAA) in *N*,*N*-dimethylformamide (DMF) (details shown in Supporting Information). Then, the CuClTAA microcrystalline thin film was obtained by spin coating. At last, Cu_9S_5 nanocrystalline conductive film was prepared by the subsequent hot plate processing. Interestingly, the crystals of molecular precursor were got by the natural evaporation of this molecular precursor solution. We determined its crystal structure through the X-ray single crystal diffraction analysis. It crystallizes in hexagonal space group (*R*3*c*), and the formula is $CuClCH_3CSNH_2$ (CuClTAA). CuClTAA crystal presents a 0D structure with a Cu_3S_3 hexatomic ring constructed by Cu^+ ion coordinated with one Cl^- ion and two TAA molecules (Figure 1a). Considering the crystal structure of Cu_9S_5 (*R*-3*m*) shown in Figure 1b (ICSD no. 41263), it still reserves the structural unit of Cu_3S_3 hexatomic ring, which is similar to that of CuClTAA (*R*3*c*), suggesting that Cu_9S_5 is decomposed from CuClTAA. The whole phase conversion process was recorded by the in situ varied temperature powder X-ray diffraction (XRD) (Figure S2). It is worth noting that digenite Cu_9S_5 (*R*-3*m*, PDF no. 47-1748) appears when the treatment temperature rises above 200 °C, indicating that the Cu_9S_5 thin film could been prepared above 200 °C. In addition, the thermogravimetry (TG) analysis of CuClTAA in Figure S3 was also consistent with the results above. The fast decomposition temperature of CuClTAA is determined as 198 °C. The actual weight loss (53.1%) in the conversion from CuClTAA to Cu_9S_5 is consistent with the theoretical weight loss (53.3%), indicating that CuClTAA has completely converted to Cu_9S_5, and our hot plate processing at 250 °C is sufficient for the forming of Cu_9S_5 nanoparticle conductive film.

Electrical conductivity significantly affects the performance of the electrode materials. Therefore, for evaluating the electrical properties of Cu_9S_5, we further develop a facile precursor solution hot inject method to prepare Cu_9S_5 nanoparticles (Details shown in Supporting Information). The powder XRD pattern, in consistent with the simulated pattern of digenite Cu_9S_5, demonstrates the phase purity of Cu_9S_5 nanoparticles (Figure S4). The scanning electron microscope (SEM) images of Cu_9S_5 nanocrystals in Figure S5 present that the morphology of the hexagonal plate is accord with the hexagonal structure of Cu_9S_5, and the size distribution ranges from 10 to 100 nm. Raman spectra and X-ray photoelectron spectra (XPS) were both measured for further investigating the characteristics of Cu_9S_5. The Raman shift in Figure S6 is 468 cm^{-1}, which is consistent with the reported value (470 cm^{-1}).[31] The Cu 2p XPS spectra in Figure S7 shows the coexistence of little Cu^{2+} and much Cu^+ in Cu_9S_5 nanocrystals.

The Hall effect, one of the most important means to obtain the materials' electrical properties, was measured on a Cu_9S_5 film with thickness 0.42 μm on a glass substrate prepared by spin-coating (Table 1). The positive Hall coefficient (5.05×10^{-4} cm^3 C^{-1}) suggests that Cu_9S_5 is a p-type compound. The high electrical conductivity (σ, 934 S cm^{-1}) demonstrates Cu_9S_5 owns an excellent hole transport ability, which is a basic requirement for a good back electrode. Notably, comparing with the traditional back contact materials, such as ZnTe:N,[32] Sb_2Te_3,[21] and Cu NW/graphene (Table 1),[33] Cu_9S_5 owns much a higher carrier concentration (N, 1.24×10^{22} cm^{-3}). In addition, it is well-known that the work function (φ) is also a very important parameter for a good back electrode. Therefore,

Table 1. Electrical Parameters of Cu_9S_5 and Several Reported Back Contact Materials

back contact materials	E_g (eV)	N (cm^{-3})	μ (cm^2 V^{-1} s^{-1})	σ (S cm^{-1})
Cu_9S_5	1.5	1.24×10^{22}	0.47	934
ZnTe:N[32]	2.2	$> 10^{20}$		0.2–25
Sb_2Te_3[21]	0.3	0.55×10^{19}	2–3	
Cu NW/graphene[33]			16.2	16.7

the φ of Cu_9S_5 was further measured by Kelvin probe method, and 1 μm Au film evaporated on a Si substrate was used as the reference (Figure 2a).[34] Compared with the frequently used metal back electrode materials, the φ of Cu_9S_5 (5.12 eV) is only 0.2 eV lower than that of Au (5.32 eV),[35] higher a bit than that of Ni (5.15 eV), and much higher than those of Mo (4.6 eV), graphite (4.6 eV), Ag (4.26 eV), and Al (4.28 eV).[21,33,36] The conductive AFM images in Figure 2b and c also suggest that Cu_9S_5 is an excellent conductive semiconductor. To highlight the conductive performance, we further measured the sheet resistance of Cu_9S_5 thin film with thickness about 300–500 nm (details shown in Supporting Information). The sheet resistance is determined as 16.6 Ω/sq by the four probe method. It is worth stressing that this sheet resistance is close to that (6–30 Ω/sq) of the commercial TCO films, like ITO, FTO, and AZO, suggesting Cu_9S_5 thin film is an excellent conductive film. According to the discussion above, we conclude that Cu_9S_5 is a p-type high work functional conductive semiconductor and p-type Cu_9S_5 nanocrystalline thin film should be a promising candidate for the back electrode of thin film solar cells.

In order to verify our conjecture, we chose CdTe thin film solar cells as the model device. Three different device structures were designed for comparing the effects after applying Cu_9S_5 thin film as the back electrode. Cells with the traditional Cu/Au thin films as the back electrode (FTO/CdS/CdTe/Cu/Au) were denoted as cell 1 for the reference, and cells with three layers of Cu_9S_5 nanocrystalline films as the back electrode (FTO/CdS/CdTe/3LCu_9S_5) were denoted as cell 2. Based on cell 2, cells with the Au film as the assistant back electrode (FTO/CdS/CdTe/Cu_9S_5/Au) were denoted as cell 3. Their device structures are presented in Figure 3a. Details of fabrication processes are described in the Supporting Information. The size of all the cells was 0.3 cm × 0.3 cm.

J–*V* characteristic curve measurements were performed to evaluate the photovoltaic efficiencies of CdTe cells (cell 1, cell 2, and cell 3) and shown in Figure 3b. The efficiency of cell 2 is 11.3%, close to that of cell 1 (11.4%), demonstrating that Cu_9S_5 film is a good replacer for the traditional Cu/Au films as the back electrode. The efficiency of cell 3 is up to 13.8% with the help of Au film, higher than that of cell 1 and cell 2. Figure 3c shows external quantum efficiency (EQE) curves of three CdTe cells. The EQE curves of cell 2 and cell 3 are similar. Comparing with cell 1, the use of Cu_9S_5 layer in cell 2 and cell 3 are mainly responsible for the differences of EQE curves in two ranges of 330–500 nm and 570–820 nm. Moreover, the using of the assistant electrode Au results in the great improvement in the range of 570–820 nm, which could result from the enhanced hole collect ability with the help of Au film. In Table 2, the FFs of cell 2 and cell 3 are both higher than that of cell 1, which should be attributed to the using of p-type Cu_9S_5 conductive film in cell 2 and cell 3.

The question is why p-type Cu_9S_5 conductive film can increase the FFs of CdTe cells? To get insight into the higher FFs in CdTe cells equipped with p-type Cu_9S_5 conductive film, we first characterized the device structure of cell 2 by the cross-sectional SEM (Figure 2d and e). The thicknesses of CdTe layer and Cu_9S_5 layer are estimated as 4–5 μm and 300–500 nm, respectively. The CdTe layer is consisted of closely packed big crystalline grains through the whole layer, and the Cu_9S_5

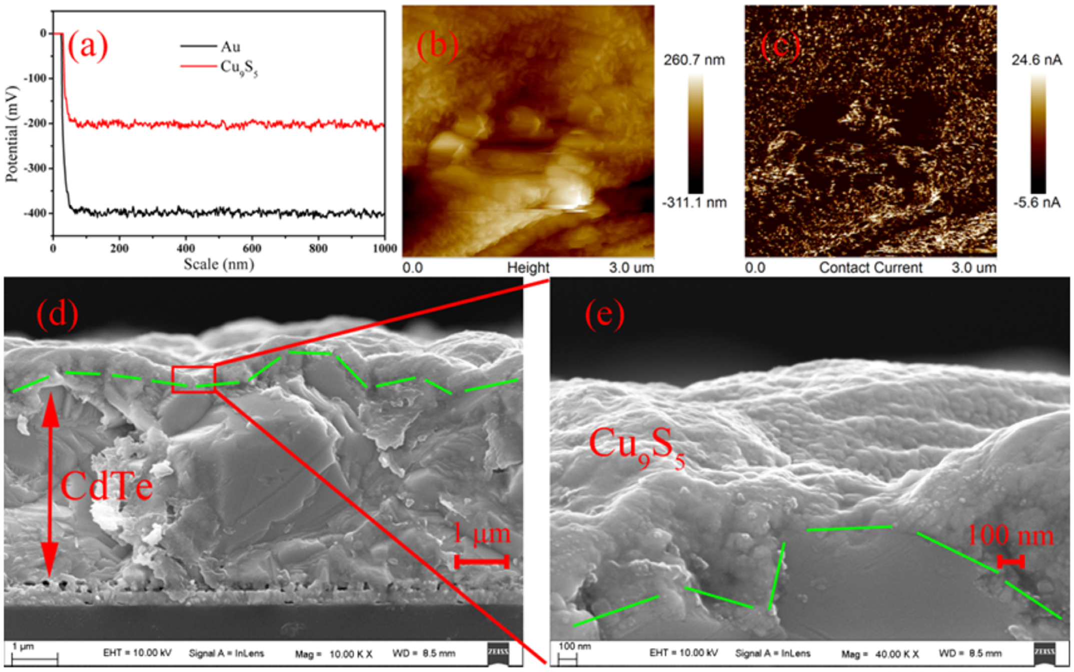

Figure 2. (a) Potential curve of Cu_9S_5 and Au measured by AFM; (b) the AFM height image of Cu_9S_5 nanoparticles; (c) the AFM contact current image of Cu_9S_5 nanoparticles; (d) the cross-sectional view of cell 2; (e) the high-magnification SEM image of Cu_9S_5 layer. The green broken lines in d and e are used to label the interface between the CdTe layer and the Cu_9S_5 layer.

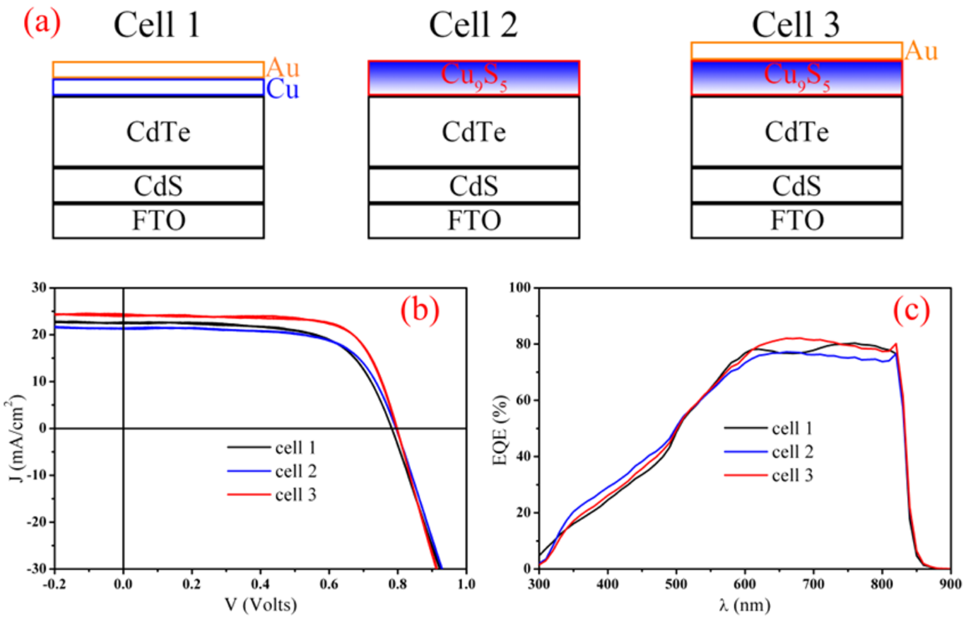

Figure 3. (a) Device structures of cell 1, cell 2, and cell 3; (b) the *J*–*V* characteristics of cell 1, cell 2, and cell 3; (c) the EQE curves of cell 1, cell 2, and cell 3.

Table 2. Photovoltaic Parameters of CdTe Cells with Three Different Device Structures

CdTe cells	PCE (%)	V_{oc} (Volts)	J_{sc} (mA cm^{-2})	FF
cell 1	11.4	0.783	22.6	0.643
cell 2	11.3	0.795	21.3	0.671
cell 3	13.8	0.797	24.0	0.721

layer is constructed with small nanocrystals with size about 100 nm (Figure 2e), suggesting that it is a nanocrystalline film. These two layers contact well, and no pinhole is observed between them. Then, the XPS depth profile was further performed to investigate the energy level structure of cell 2. The normalized atomic content of Cd, Te, Cu, and S was illustrated in Figure 4a. When the etching depth increases from 60 to 600 nm, the atomic contents of Cd and Te gradually increase, while the atomic content of Cu gradually decreases, proving the presence of successive Cu gradient doping. When the etching depth exceeds 600 nm, the atomic contents of four elements are almost unchanged, suggesting that the region

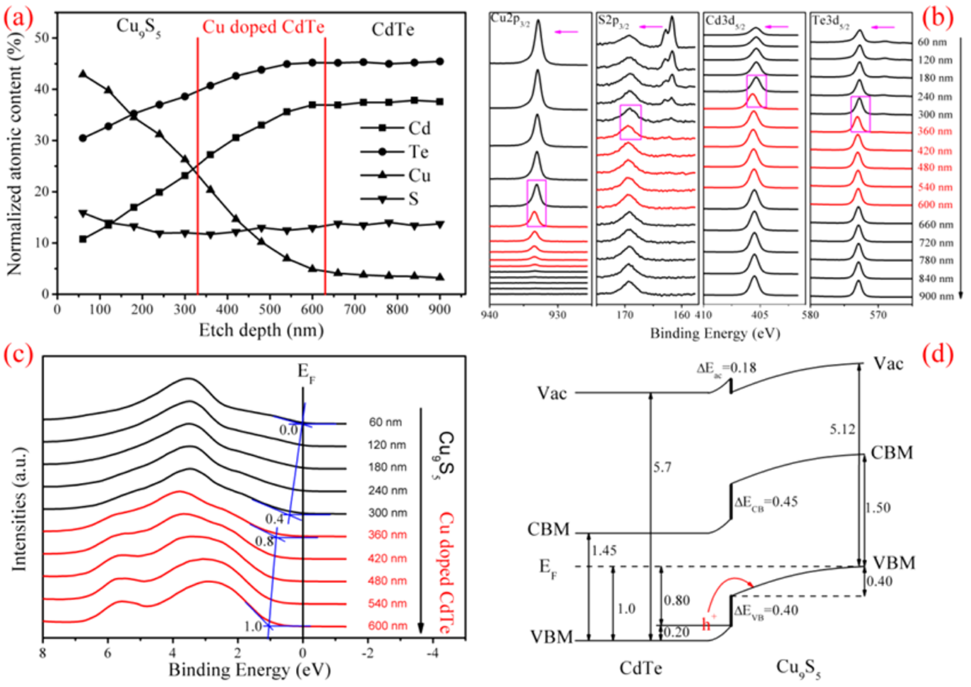

Figure 4. (a) Normalized atomic content of Cd, Te, Cu and S with the etching depth for cell 2; (b) the depth profile of Cu $2p_{3/2}$, S $2p_{3/2}$, Cd $3d_{5/2}$, and Te $3d_{5/2}$ XPS spectra with Ar^+ etching for cell 2; (c) the depth profile of normalized valence band spectra with Ar^+ etching for cell 2; (d) the energy band diagram of the CdTe/Cu_9S_5 interface. All values are given in eV.

DOI: 10.1021/acs.nanolett.5b04510
Nano Lett. 2016, 16, 1218–1223

below 600 nm is CdTe layer. Depth profiles of Cu $2p_{3/2}$, S $2p_{3/2}$, Cd $3d_{5/2}$, and Te $3d_{5/2}$ XPS spectra were presented in Figure 4b. Compared the Cu $2p_{3/2}$ XPS spectra at the etching depth of 300 and 360 nm, there is an obvious relative shift. For the S $2p_{3/2}$, Cd $3d_{5/2}$, and Te $3d_{5/2}$ XPS spectra, there is a similar relative shift, respectively. So, we could deduce that the interface of Cu_9S_5 layer and CdTe layer located between 300 and 360 nm. The depth range of Cu_9S_5 layer is 0−300 nm, which is consistent with the cross-sectional view of cell 2 (Figure 2d). In summary, the depth of 0−900 nm could be divided into three regions: Cu_9S_5 region, Cu-doped-CdTe region, and CdTe region (Figure 4a). The Cu-doped-CdTe region actually is the Cu_9S_5/CdTe interface, which is the key region needed to be focused. Investigation of the relationship between interface composition and energy level structure can help to get insight of how the interface to be able to improve the performance of thin film solar cells.

To figure out the energy level structure of both Cu_9S_5 and the Cu-doped-CdTe regions around the Cu_9S_5/CdTe interface in cell 2, the normalized valence band spectra depth profile is presented in Figure 4c. The spectrum at 600 nm is regarded as that of the undoped CdTe substrate. So we could determine the valence band maximum (VBM) of CdTe substrate as $E_{VBM} = 1.0$ eV by the linear extrapolation method. Similarly, the valence band maximum (VBM) of the Cu_9S_5 surface is determined as $E_{VBM} = 0.0$ eV from the spectrum at 60 nm. Comparing with the spectra from 600 to 360 nm (blue oblique line), it is evident that a valence band bending of $\Delta E = 0.20$ eV is determined in the Cu-doped-CdTe region owing to the Cu gradient diffusion. Notably, the extrapolation values from the spectra at 60 and 300 nm are about 0.0 and 0.4 eV, respectively, showing a much larger band bending ($\Delta E = 0.40$ eV) in the Cu_9S_5 region. This band bending could be ascribed to the result of the Cu gradient distribution in the Cu_9S_5 region (Figure 4a). So we could derive the offset between the valence band positions of CdTe and Cu_9S_5 is 0.4 eV ($\Delta E_{VB} = 0.40$ eV) at the CdTe/Cu_9S_5 interface. Using bulk band gaps of 1.45 eV for CdTe and 1.5 eV for Cu_9S_5,[37−39] the valence band offset corresponds to a conduction band offset of $\Delta E_{CB} = 0.45$ eV. Considering the work functions of CdTe and Cu_9S_5 (5.7 and 5.12 eV, respectively), we could estimate the offset of the vacuum levels ($\Delta E_{ac} = 0.18$ eV). According to the corresponding results above, the band energy diagram of the CdTe/Cu_9S_5 interface is presented in Figure 4d. It is clear that the photogenerated holes at the side of CdTe region could easily jump over the contact potential barrier of $\Delta E_{VB} = 0.40$ eV into the Cu_9S_5 region. The energy band structures of CdTe and Cu_9S_5 match very well with each other, which will benefit enhancing the hole collect and transport efficiency from CdTe layer to Cu_9S_5 layer and improving the performance of CdTe cells. Therefore, we conclude that the high FFs of cell 2 and cell 3 come from the favorable energy level matching of CdTe/Cu_9S_5 interface forming by the Cu gradient diffusion.

In addition, the short-circuit current density (J_{sc}) of cell 2 is slightly lower than that of cell 1 (Table 2), because the contact between Cu_9S_5 layer ($\varphi = 5.12$ eV) and the test electrode (stainless steel, $\varphi = 4.5$−4.6 eV) is a Schottky contact with a high potential barrier (about 0.5−0.6 eV), which is not beneficial to the collection of holes. When depositing Au assistant electrode on the Cu_9S_5 layer, the contact between Au film with Cu_9S_5 layer is an Ohmic contact with a low potential barrier (0.2 eV). So the hole collect ability was greatly enhanced and produced a highest J_{sc} and efficiency (cell 3) in the three cells (Table 2).

In conclusion, we have developed a novel p-type Cu_9S_5 nanocrystalline conductive film, for the first time, as the back electrode of thin film solar cells. Its sheet resistance (16.6 Ω/sq with thickness about 300−500 nm) is comparable to that of the commercial TCO films, like ITO, FTO and AZO. When applied in CdTe cells, p-type Cu_9S_5 conductive film produces a comparable efficiency with the traditional Cu/Au back electrode by the Cu gradient diffusion, and a higher efficiency with the help of the assistant Au film. Based on the above excellent properties, we predict Cu_9S_5 conductive film can be used as the back electrode for other thin film solar cells ($CuInS_2$, CIGSe and CZTS thin film solar cells). Moreover, Cu_9S_5 nanoparticles, prepared by a facile precursor solution hot inject method, also can be prepared into nanoparticle conductive ink or paste for more convenient and extensive applications.

■ ASSOCIATED CONTENT

Ⓢ Supporting Information

The Supporting Information is available free of charge on the ACS Publications website at DOI: 10.1021/acs.nanolett.5b04510.

Details of the experimental section, measurements and characteristics, and supplementary tables and figures (PDF)

■ AUTHOR INFORMATION

Corresponding Author

*Tel./fax: +86-755-26033200. E-mail: panfeng@pkusz.edu.cn (F. Pan).

Author Contributions

M.-J.Z. and Q.L. contributed equally.

Notes

The authors declare no competing financial interest.

■ ACKNOWLEDGMENTS

We thank financial support from the Guangdong innovative and entrepreneurial research team program (Grant Nos. 2013N080), the peacock plan (Grant Nos. KYPT20141016105435850), Shenzhen key lab (Grant Nos. (2012)780 and ZDSY20130331145131323), and Chinese postdoctoral science foundation (Grant Nos. 2015M570882).

■ REFERENCES

(1) Kim, J.; Hong, Z. R.; Li, G.; Song, T. B.; Chey, J.; Lee, Y. S.; You, J. B.; Chen, C. C.; Sadana, D. K.; Yang, Y. *Nat. Commun.* **2015**, *6*, 6391.

(2) Kim, J.; Hiroi, H.; Todorov, T. K.; Gunawan, O.; Kuwahara, M.; Gokmen, T.; Nair, D.; Hopstaken, M.; Shin, B.; Lee, Y. S.; Wang, W.; Sugimoto, H.; Mitzi, D. B. *Adv. Mater.* **2014**, *26*, 7427−7431.

(3) Zweibel, K. *Science* **2010**, *328*, 699−701.

(4) Major, J. D.; Treharne, R. E.; Phillips, L. J.; Durose, K. *Nature* **2014**, *511*, 334−337.

(5) Bi, H.; Huang, F.; Liang, J.; Xie, X.; Jiang, M. *Adv. Mater.* **2011**, *23*, 3202−3206.

(6) Lefrancois, A.; Luszczynska, B.; Pepin-Donat, B.; Lombard, C.; Bouthinon, B.; Verilhac, J. M.; Gromova, M.; Faure-Vincent, J.; Pouget, S.; Chandezon, F.; Sadki, S.; Reiss, P. *Sci. Rep.* **2015**, *5*, 7768.

(7) Bar, M.; Klaer, J.; Weinhardt, L.; Wilks, R. G.; Krause, S.; Blum, M.; Yang, W. L.; Heske, C.; Schock, H. W. *Adv. Energy Mater.* **2013**, *3*, 777−781.

(8) Wang, W.; Winkler, M. T.; Gunawan, O.; Gokmen, T.; Todorov, T. K.; Zhu, Y.; Mitzi, D. B. *Adv. Energy Mater.* **2014**, *4*, 1301465.
(9) Powalla, M.; Jackson, P.; Hariskos, D.; Paetel, S.; Witte, W.; Wuerz, R.; Lotter, E.; Menner, R.; Wischmann, W. *29th European Photovoltaic Solar Energy Conference*, Amsterdam, September 2014.
(10) Winkler, M. T.; Wang, W.; Gunawan, O.; Hovel, H. J.; Todorov, T. K.; Mitzi, D. B. *Energy Environ. Sci.* **2014**, *7*, 1029−1036.
(11) Tong, S. W.; Mishra, N.; Su, C. L.; Nalla, V.; Wu, W. Y.; Ji, W.; Zhang, J.; Chan, Y.; Loh, K. P. *Adv. Funct. Mater.* **2014**, *24*, 1904−1910.
(12) Wang, L.; Wang, H. Y.; Wei, H. T.; Zhang, H.; Chen, Q. D.; Xu, H. L.; Han, W.; Yang, B.; Sun, H. B. *Adv. Energy Mater.* **2014**, *4*, 1301882.
(13) Johnson, M. C.; Wrasman, C.; Zhang, X.; Manno, M.; Leighton, C.; Aydil, E. S. *Chem. Mater.* **2015**, *27*, 2507−2514.
(14) Yin, X.; Tang, C.; Sun, L.; Shen, Z.; Gong, H. *Chem. Mater.* **2014**, *26*, 2005−2014.
(15) Kranz, L.; Gretener, C.; Perrenoud, J.; Jaeger, D.; Gerstl, S. S. A.; Schmitt, R.; Buecheler, S.; Tiwari, A. N. *Adv. Energy Mater.* **2014**, *4*, 1301400.
(16) Gershon, T.; Shin, B.; Bojarczuk, N.; Hopstaken, M.; Mitzi, D. B.; Guha, S. *Adv. Energy Mater.* **2015**, *5*, 1400849.
(17) Zhou, H.; Song, T. B.; Hsu, W. C.; Luo, S.; Ye, S.; Duan, H. S.; Hsu, C. J.; Yang, W.; Yang, Y. *J. Am. Chem. Soc.* **2013**, *135*, 15998−16001.
(18) Panthani, M. G.; Kurley, J. M.; Crisp, R. W.; Dietz, T. C.; Ezzyat, T.; Luther, J. M.; Talapin, D. V. *Nano Lett.* **2014**, *14*, 670−675.
(19) Rioux, D.; Niles, D. W.; Hochst, H. *J. Appl. Phys.* **1993**, *73*, 8381−8385.
(20) Gessert, T. A.; Romero, M. J.; Dhere, R. G.; Johnston, S.; Duda, A. *Proceedings of 3rd World Conference on Photovoltaic Energy Conversion* 2003, A−C; pp 348−351.
(21) Abken, A. E. *Sol. Energy Mater. Sol. Cells* **2002**, *73*, 391−409.
(22) Lin, H.; Irfan; Xia, W.; Wu, H. N.; Gao, Y.; Tang, C. W. *Sol. Energy Mater. Sol. Cells* **2012**, *99*, 349−355.
(23) Lin, H.; Xia, W.; Wu, H. N.; Tang, C. W. *Appl. Phys. Lett.* **2010**, *97*, 123504.
(24) Wu, X.; Zhou, J.; Duda, A.; Yan, Y.; Teeter, G.; Asher, S.; Metzger, W. K.; Demtsu, S.; Wei, S.-H.; Noufi, R. *Thin Solid Films* **2007**, *515*, 5798−5803.
(25) Rose, D. H.; Hasoon, F. S.; Dhere, R. G.; Albin, D. S.; Ribelin, R. M.; Li, X. S.; Mahathongdy, Y.; Gessert, T. A.; Sheldon, P. *Prog. Photovoltaics* **1999**, *7*, 331−340.
(26) Tariq, G. H.; Anis-ur-Rehman, M. *Mater. Sci. Semicond. Process.* **2015**, *30*, 665−671.
(27) Yun, J. H.; Kim, K. H.; Lee, D. Y.; Ahn, B. T. *Sol. Energy Mater. Sol. Cells* **2003**, *75*, 203−210.
(28) Jaegermann, W.; Klein, A.; Mayer, T. *Adv. Mater.* **2009**, *21*, 4196−4206.
(29) Demtsu, S. H.; Sites, J. R. *Thin Solid Films* **2006**, *510*, 320−324.
(30) Donnay, G.; Donnay, J. D. H.; Kullerud, G. *Am. Mineral.* **1958**, *43*, 228−242.
(31) Kumar, P.; Gusain, M.; Nagarajan, R. *Inorg. Chem.* **2011**, *50*, 3065−3070.
(32) Späth, B.; Fritsche, J.; Klein, A.; Jaegermann, W. *Appl. Phys. Lett.* **2007**, *90*, 062112.
(33) Liang, J.; Bi, H.; Wan, D.; Huang, F. *Adv. Funct. Mater.* **2012**, *22*, 1267−1271.
(34) Palermo, V.; Palma, M.; Samori, P. *Adv. Mater.* **2006**, *18*, 145−164.
(35) Liang, J.; Lin, Q.; Li, H.; Su, Y.; Yang, X.; Wu, Z.; Zheng, J.; Wang, X.; Lin, Y.; Pan, F. *Appl. Phys. Lett.* **2015**, *107*, 013907.
(36) Demtsu, S. H.; Albin, D. S.; Pankow, J. W.; Davies, A. *Sol. Energy Mater. Sol. Cells* **2006**, *90*, 2934−2943.
(37) Wei, S. H.; Xu, Q.; Huang, B.; Zhao, Y. F.; Yan, Y. F.; Noufi, R. *38th IEEE Photovoltaic Specialists Conference (Pvsc)*, Austin, June 2012.
(38) Xu, M.; Wang, M.; Ye, T. N.; Liang, N.; Jin, L.; Zai, J. T.; Qian, X. F. *Chem. - Eur. J.* **2014**, *20*, 13576−13582.
(39) Ramli, E.; Rauchfuss, T. B.; Stern, C. L. *J. Am. Chem. Soc.* **1990**, *112*, 4043−4044.